

Article

# Impacts of Material Engineering Properties on Slope Wash and Stability in Fine-Grained Bedrock Slopes at Fossil-Bearing Sites, Badlands National Park, South Dakota, USA

Larry D. Stetler

Department of Geology and Geological Engineering, South Dakota School of Mines and Technology, Rapid City, South Dakota USA. [larry.stetler@sdsmt.edu](mailto:larry.stetler@sdsmt.edu)

\* Correspondence: [larry.stetler@sdsmt.edu](mailto:larry.stetler@sdsmt.edu)

**Abstract:** Engineering properties of bedrock materials at Badlands National Park were used to develop models for Park managers to assess slope erosion and stability for fossil resource protection. Six fully instrumented sites were used to document slope conditions. Bedrock consisted of Oligocene White River Group rocks. Bulk erosion rates correlated to grain size with silty-sandy materials producing higher mass erosion rates as a function of the silt-to-clay ratio and plastic index. Data indicated that as grain size decreased, plastic index increased leading to a decrease in erodibility. These parameters were used to construct a grain-size proxy,  $\psi$ , that was substituted for grain size,  $D$ , in Bagnold's entrainment equation and provided significant improvement in calculation of critical entrainment velocities for fine-grained materials. Hydraulic analyses of slope and pediment surface processes indicated surface roughness was a controlling factor and materials washed from rough steep slopes were effectively transported across smooth low-angle pediments with slope-to-pediment angle ratios of nearly 6:1. Slope stability modeling of ten slopes produced high factors of safety for all slopes, even under saturated conditions and was attributable to clay cohesion. All results were used to construct models that predicted years until net slope erosion equaled 2.5 cm (1 inch). Using these results, Park managers were advised to visit erosion-prone sites on a 1 to 6 year schedule, based on site geology and slope aspect, to adequately protect critical fossil resources from destruction.

**Keywords:** Badlands, erosion, slope processes, fine-grained materials, entrainment velocity

## 1. Introduction

Badlands formations are a worldwide phenomenon viewed as a group of systems with location-specific climatic and lithologic drivers [1]. Studies of badlands erosional processes in Europe since ~2000 have utilized standard field methods, erosion pins and climatic data, to quantify climatic-landform interactions, i.e., linking precipitation intensity, duration, and their variations to erosion rates [2-7]. Resulting erosion rates were determined to primarily be climatically driven and were based on trends, or changing trends, in precipitation or fluvial activity. These and additional studies [8-10] have indicated varying erosion rates ranging from negligible to ~0.5 cm/yr with higher rates up to 1.0 cm/yr [11] and >3.0 cm/yr in specific areas [12].

In the humid eastern U.S., i.e., Perth Amboy, NJ, small badlands-like morphologies resulting from erosion of clay-sand fill created badland forms that compared favorably to morphologies at

Badlands National Park (BNP) in South Dakota [13]. In South Dakota, the Tertiary White River Badlands have played a leading role in development of vertebrate paleontology in North America, beginning with the discovery and description of a titanotherium mandible [14]. This and similar work during the next 80 years led to the establishment of Badlands National Monument in 1929 and subsequent renaming to Badlands National Park in 1978, with the mission of preserving the scenic and scientific value of a portion of the White River Badlands, while remaining open and accessible to the public. Subsequent to Proulx's initial description, thousands of fossils have been collected, described, and cataloged and have served to define the Tertiary White River geologic deposits which contains one of the world's most abundant vertebrate fossil records from the late Eocene and early Oligocene [15].

Scientific research focused on erosion at BNP has been limited. Schumm [16] studied the retreat rates of miniature pediments over an ~8 year period from the mid 1950's to early 1960's. Slopes were measured by reinforcing rods driven into the ground at the base of a slope and monitoring exposure rates over the duration of the study. He used Manning's equation to determine that flow velocities generated across both slope and pediment surfaces were nearly identical. He concluded that due to the lower angle of the pediment surface and the equal flow velocity, more erosive energy was directed toward the pediment and these surfaces effectively transported all debris away from the slope. Slope retreat was replaced by development of a new pediment surface between 6 to 12 cm wide at the base of the slopes. Uniformly applying this rate over the study period, slope retreat was determined to be 0.75 to 1.5 cm/yr. Later, Stoffer [17] estimated an average erosion rate in BNP of ~2.5 cm/yr. These minimal efforts expended at BNP led to a Park-wide study to determine erosion rates at fossil-bearing sites. Initial results indicated slope retreat rates, using erosion pins, were ~2 mm during the initial 2.5 months of the project [18]. Final project results [19] showed site-wide average erosion rates were 0.41 cm/yr and ranged from 0.25 to 1.5 cm as a function of geologic formation, material engineering properties, slope aspect, and precipitation.

### 1.1 Research Goal

The BNP mission of resource preservation led to establishing the goal of constructing a fossil-site monitoring schedule. The schedule was based on statistical analysis of measured erosion rates as functions of the physical and mechanical properties of the fine-grained bedrock units in the Park. These properties were identified from analysis of collected data from six fully instrumented erosion sites located in the North Unit of BNP. Three sites were located in the east and three sites in the west (Fig. 1). Bedrock and storm-based slope wash samples were collected and analyzed to define engineering and sedimentological properties. Resulting slope wash and stability models were used to assess the effects individual properties had on erosion processes at Badlands. This paper will describe field and analytical techniques utilized to determine erosion rates and development of a new grain size proxy term used to calculate fluid entrainment velocities for fine-grained bedrock materials.

### 1.2 Regional Setting

Badlands National Park, located in southwestern South Dakota (Fig. 1), is ~80 km east of the Black Hills extending eastward another ~100 km. The Park consists of 987 km<sup>2</sup> of sharply eroded

buttes, pinnacles, and spires set within and surrounded by the largest, protected mixed grass prairie in the United States [20]. Physiographically, the Park consists of nearly flat-lying bedrock containing significant local relief due to variable erosion. The highest and lowest elevations in the Park are 1,000 m on Sheep Mountain in the west and 750 m along Sage Creek, also in the west. The largest morphological feature in the Park is the Badlands ‘Wall’ (Fig. 2), a 50 to 150 m high erosional scarp trending ~W-E for 100 km defined by steep gullied ridges with knife-like edges and pinnacles. Paleosols within the eroded sediment appear in various hues of red, yellow, and purple.

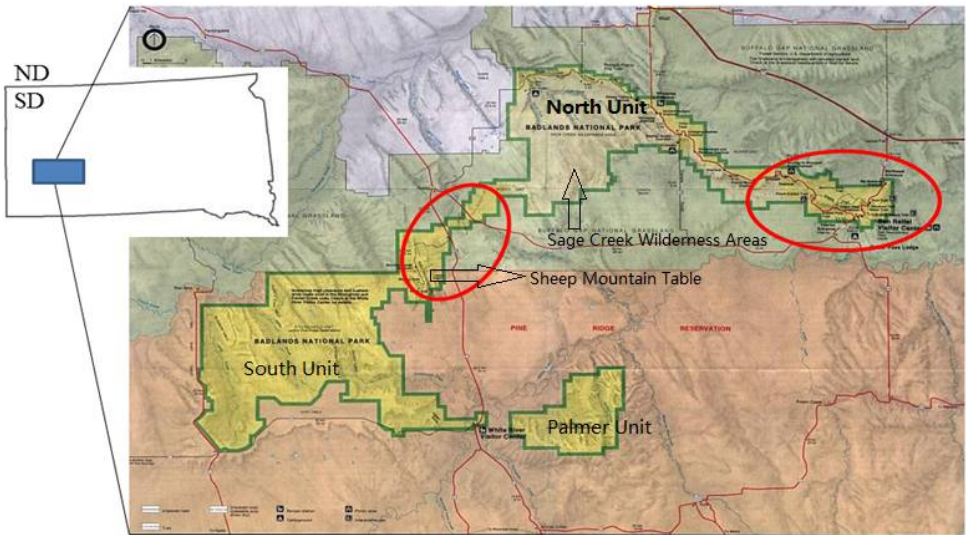


Figure 1. Badlands National Park located in southwestern South Dakota consists of North and South administrative units. Erosion sites were located within the circles at known fossil sites in the North unit.

1.2.1 Site Geology

Rocks exposed within BNP consisted primarily of the White River Group and surrounding sediments that span from late Cretaceous to mid Tertiary (early Oligocene) time [15]. Cretaceous-Paleocene rocks span a timeframe from 74-55.5 Ma. Cretaceous rocks have been divided into several facies members [17] of Campanian and Maestrichtian age. Sediments consisted of marine facies deposited in the Cretaceous Western Interior Seaway and were ~110 m thick in the Park. These rocks were primarily gray shale with abundant bentonite beds, limestone concretions, and chalk and marl beds hosting abundant marine fauna. After the sea drained away, the upper Cretaceous Fox Hills Formation marine rocks were subjected to intensive tropical weathering conditions and pedogenesis. This resulted in development of the Paleocene Yellow Mounds paleosol, a series of gold-colored alternating fine-grained sandstone and shale beds ubiquitous throughout the Park (Fig. 2).

Above the marine Cretaceous rocks, White River Group sediments were mainly fluvial in origin and consisted of poorly consolidated fluvial clay and silt deposits that included volcanoclastics and bentonite clay layers. Illite and montmorillonite have been identified as the predominant minerals [21] in these fine-grained deposits. White River Group rocks consisted of the



106 Chamberlain Pass, Chadron, and Brule Formations [15]. The caprock for the entire sequence  
 107 consists of the overlying late Oligocene Sharps Formation.

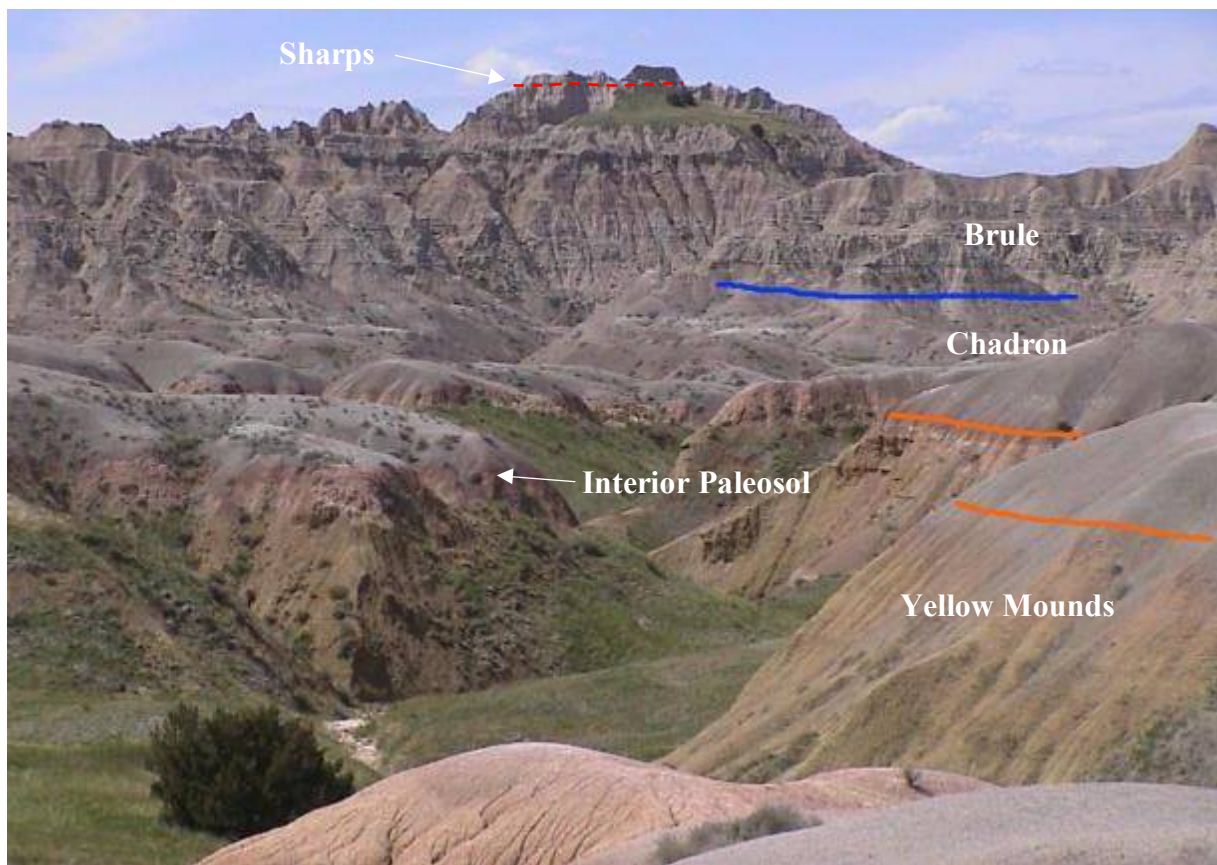


Figure 2. A complete stratigraphic sequence for Badlands geology includes: the lower-most Yellow Mounds in the upper Cretaceous-Paleocene rocks (below orange line), and the immediately overlying red Interior paleosol. Tertiary Chadron formation that are gray shales weather into low-profile haystack-like mounds (between the orange and blue lines), the steep cliffs above Chadron rocks formed in the Brule formation. Overlying cap rocks consist of Miocene Arikaree Group rocks. Brule rock form the highly gullied and steep Badlands Wall.

108 Eocene rocks represent deposition from 55.5-36 Ma. The lowermost Chamberlain Pass  
 109 Formation consisted of overbank sediments, conglomerates, and channel sands and was ~4 m thick.  
 110 Overbank fines have been weathered into the bright red Interior paleosol immediately overlying and  
 111 providing color contrast to the Yellow Mounds paleosol. Above the paleosols, Chadron Formation  
 112 rocks ranged up to 55 m in thickness and were deposited within the pre-existing valley and hill  
 113 topography. These rocks were mainly gray fine-grained claystone beds containing abundant  
 114 bentonite units that swell when wet and becomes very slippery. When dry, it forms a hard surface  
 115 marked by desiccation features resembling small aggregated popcorn-shaped mounds (Fig. 3).  
 116 Weathering of Chadron rocks produced generally low relief convexo-concave hills and were quite  
 117 distinct in occurrence and ubiquitous across the Park. Overlying Oligocene rocks were deposited  
 118 from 36-24 Ma and consisted of the Brule Formation, a mainly fluvial deposit of clay, silt, and sand  
 119 up to 140 m thick. The formation has been divided into the Scenic (Orellan) and Poleslide  
 120 (Whitneyan) members. The lower Scenic consisted of yellowish gray to buff arenaceous claystones,  
 121 paleosols, and limestone beds near the top. The upper Poleslide consisted of gray to

122 creamy-colored clay, dominated by light gray massive cliff forming sandstone that contained  
123 carbonate nodules near the top [22, 17].

124       Where erosion has removed the softer overlying clay, sandstone channels have weathered out  
125 producing distinctive columns of underlying clay capped by the protective sands, characterized by a  
126 step-and-riser topography with steep sided cliffs and sharp pinnacles (Fig. 2). Texturally, the Brule  
127 rocks ranged from lower sections that were ultra fine-grained forming low-angle slopes [23, 22] to an  
128 upper section that was more silty, thus, able to hold near vertical slopes that approach heights of 100  
129 m. It is this textural variation that leads to the formation of the many spires and pinnacles that  
130 Badlands National Park is known for.



131       Figure 3. Ice crystal expansion (below the scale) of the clay-rich Chadron Formation promotes  
132 disaggregation and formation of the aggregated popcorn-like texture (above the scale).

133       Miocene Arikaree Group rock unconformably overlying this entire sequence and form the cap  
134 rock. Locally, it consisted of the Rockyford Ash, derived from eolian ash deposits that originated  
135 from Great Basin volcanism, and the Sharps Formation consisting mainly of light gray tuffaceous  
136 sandstone and mudrock deposited in a relict topography of channels and flats.

137       Regolith was usually very thin to absent throughout the Park and ranged from unweathered  
138 bedrock to quasi developed soils ~30 cm deep [24]. Generally, Brule outcrops had thin and compact  
139 1.0 to 5.0 cm of regolith and Chadron outcrops had a loose but thicker regolith that could be >10 cm.  
140 Regolith accumulation was related to slope angle where steep slope angles hold less weathered  
141 material.

141       1.2.2 Climate Setting

142       Climate data were available for the Park from 1998 to present utilizing the Remote Automated  
143 Weather Stations (RAWS). Badlands climate is typical intercontinental characterized by hot dry  
144 summers and typically cool wetter winters. Precipitation averaged 430 mm/year ranging from a  
145 low of 249 mm/year to a high of 712 mm/year. Yearly distribution typically contained late-spring,

mid-summer precipitation peaks where single events greater than 20 mm randomly occurred. Predominate spring and summer precipitation patterns originated from the north to northwest. The average annual temperature was  $\sim 9.5^{\circ}\text{C}$  with an average annual high temperature of  $17.4^{\circ}\text{C}$  and average annual low of  $2.8^{\circ}\text{C}$ . Annual average wind speed was  $\sim 18$  kph with maximum average gusts of 48 kph. Typical spring and summer precipitation is derived from predominantly W-NW directions.

Both spring and fall seasons contained multiple weeks of diurnal freeze-thaw of the surface materials. The effects were most pronounced in fine-grained clay rocks such as the Chadron Formation. Ice crystal formation effectively splits the top few cm of depth into small spear-like slivers, disintegrating the rock into distinct small pieces that become subjective to downslope creep processes. These splits also allow rapid disaggregation to occur during subsequent precipitation wetting and slope wash processes. The typical popcorn texture (Fig. 3) of the Chadron is in part due to frost action.

## 2. Materials and Methods

Several different measurement methods were used and included stainless steel erosion pins measured using digital calipers, stainless steel rules, aluminum engineering scales, or some combination thereof, that were set at multiple locations along a slope. Full descriptions of site-layouts have been provided elsewhere [18]. Both rules and scales were imaged with a 14 MP digital camera. One m long sediment trays placed flush with the toe of monitored slopes were used to collect event-based sediment runoff from a known upslope contributing area. Precipitation data were collected at each site using a digital tipping-bucket rain gauge. Initial slope geometry was measured using a Brunton compass and tape and subsequently using 3D photogrammetry. Slope data included documented slope profile and surface changes, and surface changes around monitored fossils. Twenty-four bedrock samples were collected and analyzed for water content, grain size distribution (wet-sieve and laser particle sizing), Atterberg limits, and undrained cohesion. Slope modeling at each site, using Slide 6.0, a 2D limit equilibrium slope stability model ([www.rocscience.com/products/8/Slide](http://www.rocscience.com/products/8/Slide)), resulted in factor-of-safety (FS) determination for natural and saturated conditions.

### 2.1 Materials Testing Procedures

Slope wash sediment collected from trays at slope toes were weighed, oven dried at  $105^{\circ}\text{C}$  for 24 hours, and re-weighed to obtain water content and eroded mass. All bedrock samples were prepared by dispersing the material using sodium hexametaphosphate [25] and wet-sieving. The silt and finer fraction was determined using the Modified Wentworth system screen sizes 230 ( $63\ \mu\text{m}$ ) to 850 ( $10\ \mu\text{m}$ ) under a low constant water flow for an eight-minute period. All material exiting the  $10\ \mu\text{m}$  screen were subsequently evaluated using a laser-based liquid particle size analyzer. Additional laboratory testing of whole bedrock included determining specific gravity, Atterberg limits, and unconfined compressive strength. Atterberg limits testing resulted in determining liquid and plastic limits (LL and PL) and the plasticity index ( $\text{PI} = \text{LL} - \text{PL}$ ).

## 185 2.2 Slope Stability Modeling Procedures

186 Physical slope dimensions were measured directly and by using photogrammetry and were  
 187 used to construct model profiles for stability analysis. Each slope consisted of a single bedrock  
 188 layer that was weathered on the slope surface into a varying thickness mantle of loose, disintegrated  
 189 material that appeared much like a soil regolith. All slopes measured consisted of this weathered  
 190 surface (thickness dependent upon slope angle) and was considered less cohesive than solid  
 191 bedrock. Thus, analyses were performed using properties of normal regolith instead of bedrock  
 192 and were assumed to simulate the worst weathered case where bedrock had reduced to a loose  
 193 soil-like material on the surface, which was visual confirmed by field observation and testing.

194 Three limit equilibrium methods were utilized to solve for the factor-of-safety (FS), Bishop's  
 195 simplified method, Janbu's simplified method, and GLE/Morgenstern-Price method. The  
 196 GLE/Morgenstern method considered both force and moment equilibrium [26, 27]. A sensitivity  
 197 analysis was performed by varying the ranges of cohesion and friction angle values used in the  
 198 models to determine the influence these parameters had on slope stability.

199 Rounded convexo-concave slopes in clay-rich badlands formations (primarily Chadron rocks)  
 200 have been attributed to be primarily a function of creep processes [28, 13, 29]. Formations having  
 201 clays subjective to shrink-swell experience large volume changes with reduction/addition of water  
 202 which tends to expand the surface as weathering progresses. The resulting top layer of loose,  
 203 soil-like material has a lower bulk strength than the underlying bedrock and moves downslope by  
 204 sag and creep [24]. As a result, slopes are at, or close to, their maximum angle of stability. Such  
 205 conditions can be modeled by the infinite slope model for saturated regolith [30-32]. The general  
 206 infinite slope model [24] was used to determine the FS for homogeneous soil acting under undrained  
 207 shear strength for the two slope cases specified below.

208 Case 1: when  $d_w \geq d_r$ ,

$$209 \quad FS = \frac{UCS}{[\gamma_{sat}d_r + \gamma_w(d_w - d_r)]\sin\theta \cos\theta} \quad (1)$$

210 Case 2: when  $d_w < d_r$ ,

$$211 \quad FS = \frac{UCS}{[\gamma(d_r - d_w) + \gamma_{sat}d_w]\sin\theta \cos\theta} \quad (2)$$

212 where  $d_w$  = depth of water above the bedrock surface (depends on soil permeability),  $d_r$  = depth of  
 213 regolith (weathered) layer,  $\theta$  = slope angle determined for each slope profile,  $\gamma_{sat}$  = saturated unit  
 214 weight,  $\gamma$  = total unit weight, UCS = unconfined compressive strength, all in consistent units.

215  $d_w$  typically changes with precipitation and soil permeability which varied from  $10^{-3}$  to  $10^{-7}$   
 216  $\text{cm s}^{-1}$  for fine sand, silt, and mixtures of sand, silt, and clay to  $<10^{-7}$   $\text{cm s}^{-1}$  for homogeneous clay [33].  
 217  $d_r$  was estimated based on Howard [24] and visual estimations from the field that were consistent  
 218 with these values. The slope angle was a measured value and remained invariant for each  
 219 individual slope.  $\gamma_{sat}$ , and  $\gamma$  were obtained from laboratory work. Using equations (1) and (2), FS  
 220 values were calculated for slopes at Badlands.

## 221 3. Results



Table 1 contains the results of the materials testing for Badlands formations. These data were utilized to evaluate slope erosivity and stability, the latter by constructing stability models for assessing effects that water content, cohesion, and internal friction angle had on FS analysis.

Table 1. Average geomechanical properties of slope wash and bedrock samples obtained from laboratory tests from each of the six erosion sites.

Site	Member	Water Content %	Wet Sieve		Mean Size μm	Unit Weight		Undrained Cohesion kPa	Atterberg Limits			SG gcm <sup>-3</sup>
			% Passing			Dry	Wet		LL	PL	PI	
			230	850								
BL-01	Poleslide	8.21	96.2	53.5	16.6	14.7	18.1	37.8	63.2	30.0	33.2	2.58
BL-02	Scenic	4.64	79.2	43.0	33.0	17.3	19.9	59.9	43.2	19.0	24.2	2.56
BL-03	Scenic	6.41	86.6	52.8	21.1	16.4	19.3	47.5	49.7	23.4	26.3	2.58
BL-04	Scenic	8.68	97.9	63.5	12.6	14.7	18.1	65.9	86.0	31.0	55.1	2.57
BL-05	Peanut Peak	12.18	98.9	84.0	8.1	13.7	17.3	64.0	128.0	43.1	85.0	2.68
BL-06	Scenic	11.40	96.2	63.0	12.7	16.6	18.9	82.7	95.4	27.4	68.0	2.57

### 3.1 Physical and Engineering Properties

The finest-grained material identified was the clay-rich gray-green mudstone from the Peanut Peak member of the Chadron Formation (Site BL-05) with 84% passing the 850 screen (10  $\mu\text{m}$ ). It had the smallest averaged mean diameter (8.09  $\mu\text{m}$ ), the highest Atterberg limits, highest initial water content, and smallest unsaturated and saturated unit weight. Conversely, the coarsest material was the Scenic member of the Brule Formation at Site BL-02 which consisted of gray silty sandstone with 43% of the material passing the 850 screen. It had the largest averaged mean diameter (33  $\mu\text{m}$ ), the lowest Atterberg limits, and largest unsaturated and saturated unit weight. Across the North Unit, the 3 sites in the east (BL-01, 0-2, 0-3) were coarser-grained (average 23.6  $\mu\text{m}$ ), had the lowest Atterberg limits (average PI 27.9), largest unit weights, and the smallest undrained cohesion. The 3 sites in the west (BL-04, 0-5, 0-6) were finer-grained (average 11.1  $\mu\text{m}$ ), had the greatest Atterberg limits (average PI 69.3), smallest unit weights, and the greatest undrained cohesion. One likely reason for the distinctions in parameters, even in the same member unit, was that the regional dip of the formations ( $\sim 2\text{--}3^\circ$  E) exposed different portions of the formations from west to east. These data trends were consistent with the collected erosion data.

Specific gravity values were determined using the eroded materials collected from the sediment trays following ASTM methods [34]. Scenic and Poleslide members were  $\sim 2.57 \text{ gcm}^{-3}$  and the Chadron was 4.7% higher at  $2.68 \text{ gcm}^{-3}$ . SG values had a standard deviation of 0.049.

### 3.2 Slope Erosivity and Stability

Slope profiles represent physical process responses between the forces generated on the slope driving downslope motion of bedrock and loose debris and the engineering properties of the slope materials resisting motion. Forces of erosion may be generated by either fluid or gravity. Howard [24] described erosional processes acting on Badlands slopes and divided them between wash (fluid)



and mass wasting (gravity). Wash processes primarily occurred from rainstorms including runoff and splash erosion. Mass wasting resulted mainly from unstable regolith or bedrock moving downslope under gravity including creep, sliding, and flows [17]. Both situations were modeled during this study using engineering parameters for exposed bedrock at erosion sites.

### 3.2.1 Erosivity From Wash

Slope wash produces eroded sediment as a function of mass and depth of flowing water, slope angle and length, and the properties (size, shape, mechanical attributes) of particles resting on the slope. For non-cohesive particles, downslope transport occurs when the critical shear stress,  $\tau_{cr}$ , exceeds material strength and is dependent upon grain size,  $D$ , i.e.,  $\tau_{cr} \propto D$  [35].  $\tau_{cr}$  is a difficult parameter to quantify for cohesive silt and clay (<16  $\mu\text{m}$  diameter) [36], in that erosion resistance is increased above that for granular material (0.1 – 10 mm) and depends on cohesive attraction (valency charge forces) generated between adjacent particles rather than on the physical parameters of the particles themselves. Thus, a critical shear stress does not exist in the same meaning as for non-cohesive materials.

At Badlands, slopes <35–40° consisted uniformly of weathered bedrock materials (regolith) that mantled slopes to depths of up to ~30 cm but were typically thinner. The material appeared loose, fluffy, and airy with significant cohesion, particularly in finer-grained units. When wetted, slope wash physically removed and transported some of this material toward the slope toe depositing it as a type of fan, or pediment (also noted by others) [13, 16, 22, 24] that was typically smooth and compacted. The same runoff was likely to carry some portion of the eroded material away from the slope resulting in a net lateral slope retreat over time.

Physically, the erosional mechanism for regolith proceeds as a grain-fluid interaction. Wetting of the regolith effectively disaggregated the non-lithified fine-grained bedrock particles and slope wash consisted of individual particles, not aggregated clumps. This process produced the smooth and compacted pediment surfaces noted by Schumm, Smith, and Howard and were observed during the present study. Additionally, eroded materials collected in sampling trays consisted of disaggregated sediment with occasional aggregated clumps (Fig. 3). These clumps were always attributable to non-precipitation event gravity falls and were easily distinguished from slope wash as they were always resting on top of the sediment in the tray and not incorporated into it. Immediately after precipitation events and until slopes desiccated, no collected eroded materials were aggregated. Thus, for these bedrock materials, slope wash occurred mainly by entrainment and transport of individual silt and clay particles.

Utley and Wynn [37] evaluated wash processes for cohesive materials using a method that related critical shear stress,  $\tau_{cr}$  (Pa), to several soil properties including PI.  $\tau_{cr}$  was then used to determine a soil erodibility coefficient,  $k_d$  ( $\text{cm}^3/\text{N-s}$ ):

$$\tau_{cr} = 0.16(PI)^{0.84} \quad (3)$$

$$k_d = 0.2\tau_{cr}^{-0.5} \quad (4)$$

$k_d$  is an indicator of erosion resistance where the smaller the value, the greater the erosional resistance. Mechanically, as PI increased, cohesive forces between adjacent particles increased (Fig.

4A) requiring higher shear stresses to mobilize the grain which resulted in an increased resistance to erosion. PI is also reflective of the silt to clay ratio, S:M, based on the sieve analysis and defined as the ratio between the percentage of grains at 60% and 10% finer, in that smaller ratios indicate greater clay content and an increased PI value. On figure 4A, the coarse-grained material (closed symbols) had a S:M of 0.19 and the fine-grained materials (open symbols) had a S:M of 0.05. These data indicate that higher clay content resulted in a lower S:M ratio, an increased PI, and a decrease in  $k_d$ , resulting in increased erosion resistance.

Resistance to erosion was determined by directly comparing calculated  $k_d$  values to the mass flux,  $\dot{m}$  ( $\text{gm}^{-2}$ ), of eroded sediment from monitored slopes (Fig. 4B). Mass flux was determined by dividing the total mass (g) of materials collected in a sediment tray by the contributing slope area ( $\text{m}^2$ ). These results suggest that erosivity was a function of grain size, i.e., finer-grained materials were less erosive than coarser-grained materials and these relations represent engineering properties of the materials.

As PI decreased,  $k_d$  increased logarithmically in response to a decrease in erosion resistance. Increasing S:M ratios resulted in greater amounts of slope wash, however, mass flux decreased logarithmically through the process. This suggests the existence of an upper limit to PI effects for erosion resistance and lies most likely in the LL, itself a function of the S:M ratio. These results suggested that erodibility assessment for cohesive materials are possible if engineering properties of the material are known, particularly PI. In most cases, attaining engineering properties for representative materials is a rapid process and has been used effective for mitigation efforts rather than determining site-specific erodibility conditions. At the least, stability results based on materials engineering properties would enhance site selection where long-term monitoring may be required. Although these results appear to be robust for calculating erosivity potential, they do not provide an actual value for  $\tau_{cr}$ . Therefore, a method for determining  $\tau_{cr}$  for cohesive materials is needed.

Hjulström [38] and Shields [39] demonstrated that erosion (entrainment) resistance increased for cohesive materials above those of granular non-cohesive materials. Shields used dimensionless parameters for grain size and shear stress and determined regions of motion and no motion. Hjulström's diagram (Fig. 5) segregated process-based regions from erosional to depositional conditions for grains as small as 0.001 mm (1  $\mu\text{m}$ ). Velocities required to entrain grains ranged widely between unconsolidated and consolidated materials and was defined as the region between the dashed lines. For example, an unconsolidated particle of size 0.01 mm would move with a velocity of  $\sim 30 \text{ cms}^{-1}$  rising to  $>100 \text{ cms}^{-1}$  if it were consolidated. Although equations exist to determine entrainment velocities for granular materials  $>0.1 \text{ mm}$ , few equations exist for clay particles.

Using figure 5, average-sized particles for Badlands formations require fluid entrainment velocities between  $\sim 70 - 300 \text{ cms}^{-1}$ . The standard equation used to calculate critical entrainment velocity,  $u_{*c}$ , for granular materials was developed by Bagnold [40] and has been widely used:

$$u_{*c}^* = k \sqrt{\left(\frac{\sigma - \rho}{\rho}\right) g D} \quad (5)$$

where  $k$  = fluid coefficient ( $\sim 0.2$  for water),  $\sigma$  = particle density,  $\rho$  = fluid density,  $g$  = gravitational constant, and  $D$  = mean particle diameter. This equation is valid for particles  $> 0.1$  mm ( $100\ \mu\text{m}$ ) and, thus, cannot be used directly for the fine-grained materials at BNP. For smaller particles, entrainment velocities increase as a function of decreasing grain size attributable to chemical force attraction between particles, or cohesion, and fundamental particle shape changes. The complexity of the particle force attractions vs. motive forces makes this problem non-trivial.

That  $k_d$  has been shown to correlate to material engineering properties suggests these same properties may be useful to construct a grain size proxy for use in equation (5). For cohesive soils, PI has been shown to be a function of grain size and to control erosion resistance through  $k_d$  (Fig. 4). Thus, a proxy grain size parameter,  $\psi$ , was developed based on the engineering parameters of cohesive materials. The relative strength of these parameters relies on the physical distribution of particles represented by the S:M ratio. The grain size proxy was determined as

$$\psi = \frac{PI \cdot C}{S:M} \quad (6)$$

PI and cohesion hold the material together by generating bulk strength properties and are primarily related to the small particle sizes for clay-rich material. Materials defined by small S:M ratios provide conditions where grain platelets arrange in a more stacked configuration with decreasing size where increased molecular force interactions on grain edges and surfaces dominate. Wetting and hydrating the particles will further increase attractive forces [41]. The combined effect is to generate material strength that is reflected by increases in PI and cohesion. Changes in the grain-size distribution alters this function. Materials having a larger S:M ratio leads to decreased grain-to-grain contact and reduced molecular charge attraction. The more granular the mixture becomes, the less bulk strength the material has and is reflected by lower PI and cohesion. The effect of the S:M ratio provides the basic physical mechanism that defines erodibility of fine-grained materials.

Substituting  $\psi$  as a proxy for the mean grain diameter,  $D$ , in (5) and plotted on the Hjulström diagram (Fig. 5) indicated that Badlands materials behave primarily as consolidated, i.e., cohesive, material. Decreases in the S:M ratio increased bulk strength increasing erosive velocity in fine-grained clay-dominant materials. Materials that contained larger S:M ratios (higher silt content) behaved oppositely. The range of critical velocities required to entrain these materials were calculated to be between 75 to 300  $\text{cm s}^{-1}$ . Not only does  $u_c^*$  plot correctly in terms of material type but is it significantly correlated to  $k_d$ , the resistance parameter (Fig. 6).

For the range of particle-size distributions for Badlands slopes, entrainment velocities were calculated using:

$$u_c^* = 2000e^{-25k_d} \quad (7)$$

where  $k_d$  is based on PI. This equation remains valid over the range of PI values for the materials that were tested.

Schumm [16] used Manning's equation for open channel flow to evaluate velocity on both slopes and pediments at BNP. In his analysis, the flow depth was assumed to be the same on slopes and pediments thereby eliminating it as a parameter in the equation. The result was a relative velocity measure,  $V_r$ :

$$V_r = \left( \frac{1.49}{n} \right) S^{0.5} \quad (8)$$

where  $n$  = roughness coefficient and  $S$  = slope inclination. Roughness values were selected from Chow [42] and were 0.06 and 0.02 for the slope and pediment, respectively (slopes were rougher).

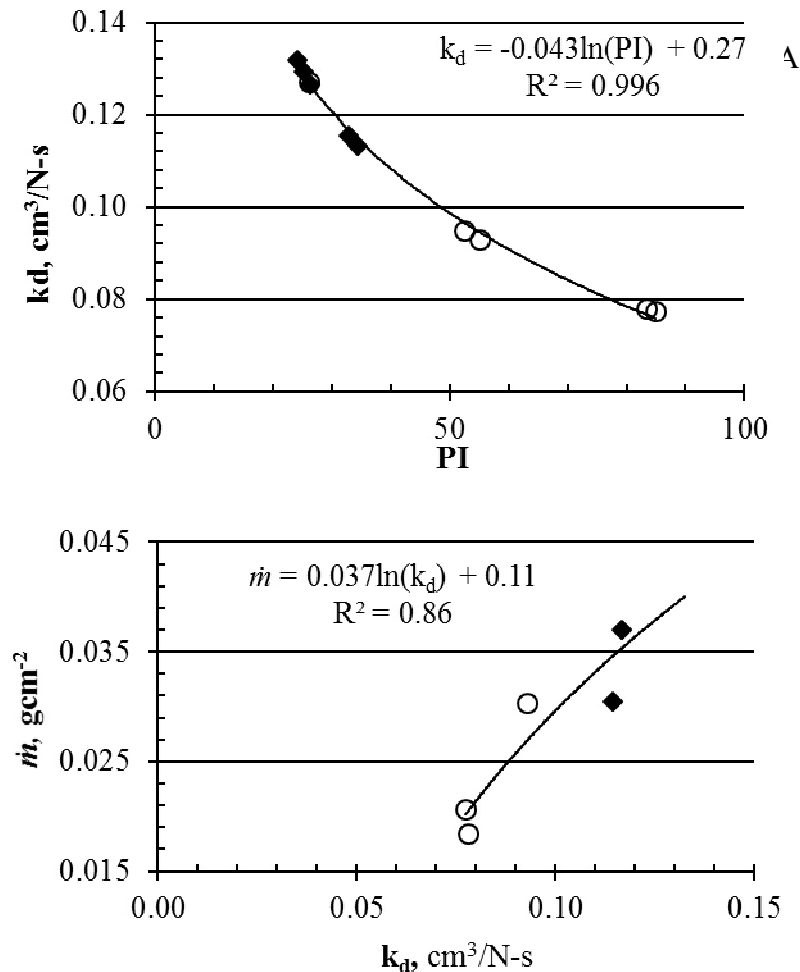


Figure 4. A) Erosion resistance correlates to PI indicating fine-grained materials (open symbols) have greater erosion resistance (lower  $k_d$ ) than coarse-grained material (closed symbols). B) Sediment mass flux from slopes support the use of the erodibility coefficient based on Atterberg Limits testing. Slopes in the western Badlands (open symbols) were finer-grained than those in the eastern Badlands (closed symbols) and yielded less sediment mass flux.

All measurements were averaged and  $V_r$  was 23 and 24 for slopes and pediments, respectively. That  $V_r$  was the same on both surfaces was a result of decreasing roughness on the pediment being compensated by a corresponding decrease in the slope angle away from the slope.



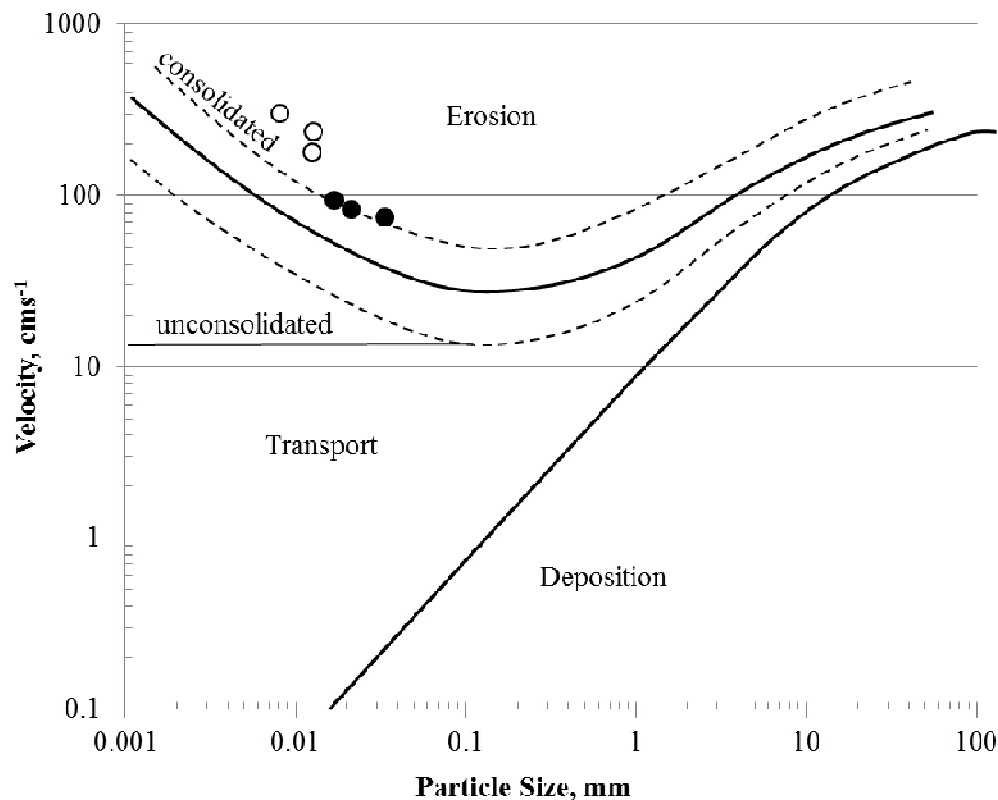


Figure 5. Hjulström's diagram relates processes to velocities. Particles <0.1 mm require higher entrainment velocities as functions of grain size, shape, and particle attractive forces. Badlands materials are plotted that were determined using the grain-size proxy. Open symbols had a smaller S:M ratio and were more clay-rich than closed symbol materials that had a larger S:M ratio.

Using measurements of slopes and pediments obtained from 3D photogrammetry and the same roughness values used by Schumm,  $V_r$  comparisons were calculated. Average relative velocity values were the same on slopes and pediment surfaces and were 26. Although the angle ratio between slope and pediment was 5.8, the decrease in roughness on the pediment produced a consistent velocity and energy condition to effectively transport particles across the lower angle surfaces. Sediment delivered to the toe of the slope, was effectively transported by efficiency of flow energy across the pediment and in time resulted in a general lateral slope retreat. This process was facilitated by the disaggregation of the bedrock when wetted and Atterberg limits were above the LL and particle strength was reduced. Sediment transport processes were activated during runoff events and the more precipitation received on a slope, the higher the mass flux of sediment (Fig. 7). These data show net slope retreat for 2 adjacent slopes at site BL-01 as functions of precipitation. Slope retreat values were measured as mm of erosion (surface lowering) between successive measurement periods. Slope retreat was accelerated during summer 2011 during a relatively large precipitation event. Slope movement was mostly subdued until the next precipitation event in spring 2012. However, retreat was less in response to a lower intensity event. These data also show effects of slope aspect, or direction of the slope to the direction of the precipitation. Slope 05R was south-facing and was shielded from the primary intensity of the

precipitation from the northwest. The north-facing slope, 06R, received the full impact of the precipitation and produced greater sediment mass flux and larger net slope retreat. These slopes were separated by an ~2 m wide pediment and were in the same units of the same formation. These processes acting through time are responsible for the generation of the low-angle smooth pediment surfaces leading away from slopes that are ubiquitous features across the Badlands.

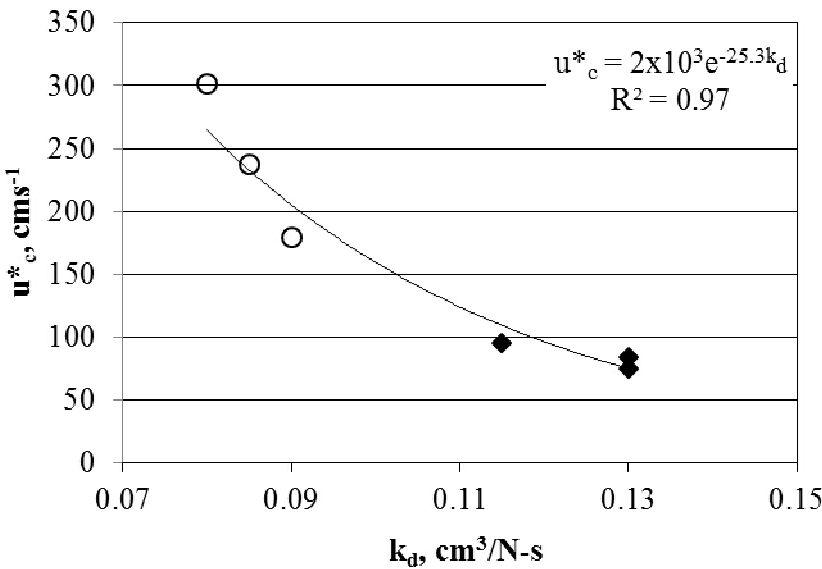


Figure 6. Soil erodibility coefficient,  $k_d$ , and critical shear velocity,  $u^*_c$ , based on  $\psi$ , the grain-size proxy, hold physical significance for fine-grained materials and are both anchored by engineering properties of the materials. Open symbols have lower S:M ratios.

3.2.2 Slope Stability Modeling

Landslides represent normal geomorphic processes indicating instability in slope profiles or force balance. Acting through time, these processes produced equilibrium slope profiles as a function of slope material, slope height, and climate intensity [22]. At Badlands, landslides have been mapped in the Cedar Pass, Sage Creek, and Norbeck Pass areas [23] that are contained in the red circles on figure 1. Howard [20] showed that mass wasting rates rapidly increased when slope gradients approached the limiting slope angle of ~34-36°. Slope angles greater than the limiting value typically occur in Brule formation rocks which forms the Badlands Wall (Fig. 2). Brule rocks contain sufficient silt and fine sand that with the clay needed to provide cohesive strength has the inherent ability to weather into the characteristic tall and steep sloped forms [22]. Expectedly, the greatest number of landslides in the Park have been identified in the Brule. Instability leading to failure has occurred due to tension failure from both desiccation and/or undercutting.

Smith [22] also suggested creep-like movement predominated on lower gradient slopes, such as in Chadron formation slopes that typically have maximum angles ~26° (Fig. 2). Grain size distributions indicated Brule rocks contained 50% of the grains >25  $\mu\text{m}$  diameter and were the coarsest units identified and also contained the tallest and steepest (~52°) slopes that were measured during the study. Chadron rocks were the finest-grained units identified with 50% of the grains >4.6  $\mu\text{m}$  and ~80% of the grains <10  $\mu\text{m}$ . These rocks contained the greatest cohesion but due to a

greater clay content had the least steep slopes and weathered into characteristic low-profile  
convexo-concave mounds.

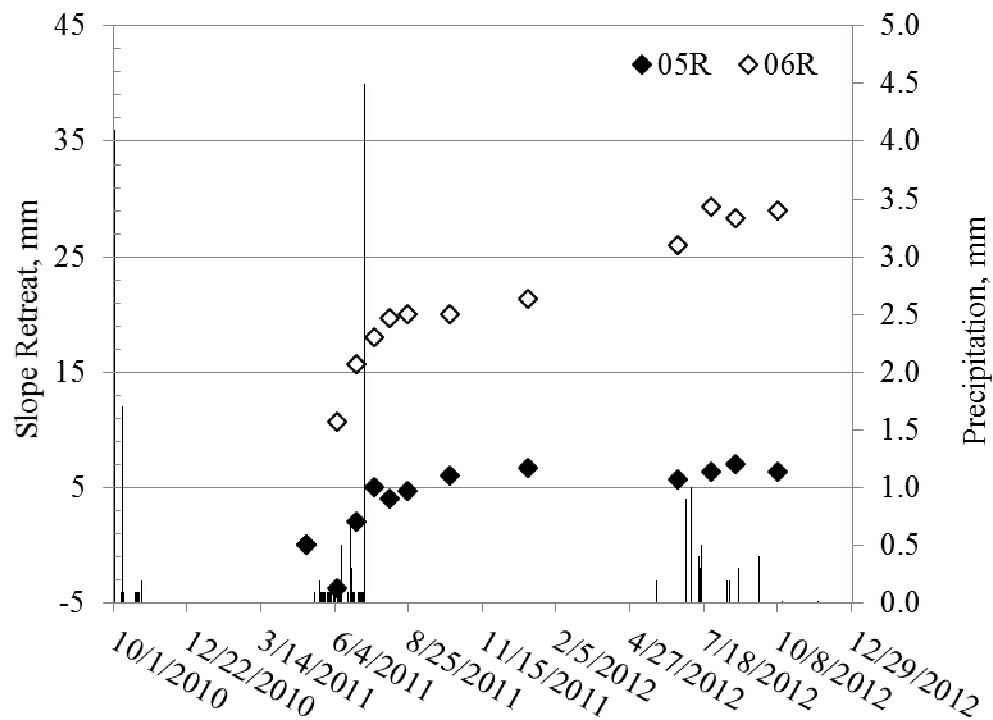


Figure 7. Slope retreat data for 2 slopes at site BL-01 for approximately 2 years. Slope 05R utilized erosion pins and slope 06R utilized steel rules. Precipitation is shown as lines.

Slope stability modeling (equations 1 and 2) requires a known material shear strength. Typically, saturated clays have no internal friction and in undrained conditions, undrained cohesion,  $c_u$ , can be considered equal to shear strength. Thus, the strength test results provided  $c_u$  and unconfined compressive strength,  $q_u$ , was determined using:

$$q_u = \frac{c_u}{2} \quad (8)$$

$q_u$  was subsequently used in the FS equations for slope stability assessment.

Stability analysis were conducted using three limit equilibrium methods (section 2.2). The physical setting was based on the measured slope profile. Model parameters were determined either through direct material testing or parameter modeling using test results. All FS results from all three methods were similar indicating no significant differences between methods. Variance between method results were also provided from the modeling and were zero for coarse-grained sites (BL-01 through BL-03) and ranged from zero to 9 for the fine-grained sites (BL-04 through BL-06). FS and variance were unusually high for slopes BL-06 since these were low angle slopes ( $<10^\circ$ ). Slopes BL-04 through BL-06 had higher FS values for 2 reasons: 1) grain-size distributions on these slopes were significantly skewed toward finer grains (50%  $<10 \mu\text{m}$ ), and 2) increased cohesion (high PI values) of the materials on the slope enhanced erosion resistance. Lowest FS was obtained in all cases under a surface water table and saturated conditions. Even under these saturation condition, no slopes contained a FS  $<$  threshold conditions. Slopes closest to failure

conditions were BL-01 and was located in an area of ubiquitous failures in Brule rocks, mainly from a combination of saturation and tension failure. Tallest modeled slopes were ~5 m high and slope failures began to appear in slope with heights above ~20 m.

Sensitivity analysis for the 10 modeled slopes indicated that slope stability was more sensitive to cohesion than angle of internal friction. Varying cohesion between 0 and 50% of the true value resulted in FS variations from 11 to 31%. Conversely, variations in internal angle of friction between 0 and 50% of the true value resulted in FS variations from 0 to 1.42%.

Material properties were mainly derived from the fine grain size, particularly the S:M ratio. Increasing the clay content increased cohesion thereby limiting variations in FS values. These FS variations were more pronounced for the coarse-grained materials at sites BL-01 through BL-03 where FS changes averaged 22%. For these coarse-grain dominate slopes, variations in the clay content changed cohesion enough to result in a high variability in FS. For fine-grained slopes (BL-04 through BL-06), variations in clay content had a more subdued effect on cohesion owing to the overall finer textured materials and the result was a subdued variation in FS values. These sites had an average FS change of 14%, a net decrease of 64% in average FS variation between the coarse- and fine-grained sites.

### 3.3 Site Monitoring Schedule

Results of net slope retreat from 10 monitored slopes as functions of slope angle, aspect, and precipitation were modeled to produce a first-cut suggestion for a site monitoring schedule. Multiple regression models were used to determine the most sensitive modeling variables that controlled erosion and could be used to predict future site monitoring. Slope aspect was the most critical factor for determining erosion potential and was followed by formation, or bedrock type (Table 2). An erosion ratio was calculated between the most erosive condition and all other slopes. For example, for slope aspect, the north-facing slopes had the highest erosion rate and south-facing slopes had the least. The erosion ratio for north-facing slopes was 1.0 and for south-facing slopes was 0.2. Thus, slopes having a north aspect were ~five times more erosive. The same procedure was used for formation and location. These results indicated that the Poleslide was the most erosive formation and given the equal distribution of formations throughout the study region, the location erosion ratio was essentially the same.

Accordingly, slope aspect was determined to be the most critical parameter to use in the site visitation schedule. Regression models were used to determine the erosion rate per year and the number of years for a slope to experience 2.54 cm of erosion. Years between site visits vary from ~1 year for north-facing slopes to ~6 years for south-facing slopes. Park officials will also be required to assess fossil types and protection standards when making final decisions for site visits.

## 4. Conclusions

Landforms at Badlands National Park have developed through long-term interactions of climate and geology. Material properties of the exposed formations governed erosional processes and were highly dependent on grain-size distributions and mineralogy within stratigraphic units. Variations in the silt to clay content were determining factors for erosion resistance of each formation. Increased clay content has been determined to increase PI, unit cohesion, and increase



erosion resistance. Increased silt content resulted in lower PI and decreased unit cohesion based on the S:M ratio. However, the added mechanical stability from increased silt enables near vertical cliffs to form, although these units have a decreased resistance to erosion and generate a greater mass flux than the clay-dominate units.

Table 2. Erosion modelling results for slope aspect, bedrock formation, and location in the Park. The erosion ratio is based upon the most erosive parameter. Suggested years between visits were normalized on ~years for 2.54 cm of erosion to occur.

Aspect	R <sup>2</sup>	Retreat		
		mm	Ratio	Yr
N	0.88	39.8	1.0	1.3
S	0.47	8.9	0.2	6.1
NW	0.66	16.5	0.4	3.1
SE	0.86	12.0	0.3	5.5
SW	0.71	23.0	0.6	2.2
Formation				
Poleslide	0.59	25.0	1.0	
Scenic	0.78	18.1	0.7	
Peanut Peak	0.48	15.1	0.6	
Location				
East	0.71	20.1	1.0	
West	0.73	17.9	0.9	
All Sites	0.72	19.1	1.0	

Analysis of material engineering properties of the bedrock has resulted in development of a grain-size proxy indicator,  $\psi$ , based the plasticity index, unit cohesion, and the S:M ratio. This parameter was successfully substituted into Bagnold’s entrainment equation to calculate critical threshold velocity that was plotted on a Hjulström diagram. These results indicated that valid entrainment velocities were able to be calculated based on the engineering properties of a fine-grained material. Plasticity index was observed to positively correlate to an erosivity resistance factor,  $k_d$ , and as PI increased, the erosion resistance of the material increased, reflected as a decrease in  $k_d$ . These data and results suggested that slope erosion processes functioned as individual particles were disaggregated from bedrock during wetting and were transported downslope as sheetwash. Loose sediment material delivered to the toe of the slope produced a low-angle pediment leading away from the slope. Variations in surface roughness between slope and pediment was responsible for maintaining high velocity flows on the pediment that carried sediment away from the slope and prohibited sediment accumulation at the toe. The result was a general retreat of the slope through time producing an equilibrium slope profile based on geomechanical and mineralogical attributes of the units being weathered. Thus, equilibrium slope profiles at Badlands have developed as a direct response to the S:M ratio.

Geomechanical properties of the bedrock on all slopes produced stable profiles even under saturated conditions. Modeled slopes were sensitive to cohesion and contained up to 31% variance in FS under a 50% change in cohesion. Slope instability was visually observed where steep slopes exceeded ~20 m in height and become unstable from desiccation and tension fractures at the top of

the slope and/or undercutting at the toe. None of the slopes modeled met either condition and were mechanically stable.

All results were used to develop a paleontological monitoring program for BNP managers based on the time (years) calculated for net slope erosion to equal 2.5 cm. The schedule was based on an erosion ratio that indicated erosion potential. North-facing slopes were ~5 times more erosive than south-facing slopes. This led to suggested site visits for north slopes every year and every 6 years for south slopes. Overall, coarser-grained rocks, such as Brule rocks, were 1/3 more erosive than fine-grained rocks. Thus, paleontological monitoring of fossil resources was determined to be highly variable but somewhat predictable. Erosion at BNP remains somewhat unknown given the limited scope of this study but was shown to be dependent upon the physical setting, bedrock properties, and the climate.

**Acknowledgments:** This research was conducted under a research grant from the US Department of Interior, National Park Service utilizing a Cooperative Ecosystems Studies Unit (CESU), Task Agreement J1300110051. Continued field access granted by Badlands National Park through 2018. Data that are not location specific or sensitive to the Park Service are available from the author.

## References

1. Nadel-Romero, E.; Torri, D.; Yair, A.; Roo, A. Eds.; Updating Badlands Research. *Catena* 2013. 106, 1-122.
2. Faulkner, H. Connectivity as a crucial determinant of badland morphology and evolution. *Geomorphology* 2008. 100(1-2), 91-103.
3. Cras, A.; Marc, V.; Travi, Y. Hydrological behavior of sub-Mediterranean alpine headwater streams in a badlands environment. *Jour Hydrol* 2007. 339(3-4), 130-144.
4. Appel, J. K. Characterisation of badlands and modelling of soil erosion in the Isábena watershed, NE Spain, Germany. M.S. thesis, University of Potsdam, 2006.
5. Clarke, M.L.; Rendell, H.M. Process-form relationships in Southern Italian badlands: erosion rates and implications for landform evolution. *Earth Surf Proc Landforms* 2006. 31, 15-29.
6. Cantón, Y.; Domingo, F.; Solé-Benet, A.; Puigdefabregàs, J. Hydrological and erosion response of a badland system in semiarid SE Spain. *Jour. Hydrol* 2001. 252, 65-84.
7. Regüés, D.; Guardía, R.; Gallart, F. Geomorphic agents versus vegetation spreading as causes of badland occurrence in a Mediterranean subhumid mountainous area. *Catena* 2000. 25, 199-212.
8. Alatorre, L.C.; Beguería, S. Identification of active erosion areas and areas at risk by remote sensing: an example in the Esera—Isabena watershed, the Central Spanish Pyrenees. *Geophys Res Abs* 2009. 11, 2665.
9. Seta, D.M.; Del Monte, M.; Fredi, P.; Lupia Palmieri, E. Gully erosion in central Italy: Denudation rate estimation and morphoevolution of Calanchi and Biancane badlands. Proceedings of the IV International Symposium on Gully Erosion. Pamplona, Spain, 2007. J. Casali, R. Giménez. Eds.
10. Martínez-Carreras, N.; Soler, M.; Hernández, E.; Gallart, F. Simulationg badland erosion with KINEROS2 in a Mediterranean mountain catchment (Vallcebre, Eastern Pyrenees). *Geophys Res Abs* 2005. 7, 08736.
11. Saynor, M.J.; Loughran, R.J.; Erskine, W.D.; Scott, P.F. Sediment movement on hillslopes measured by caesium-137 and erosion pins. Proceedings of the Canberra International Symposium. Canberra, Australia, 1994. Int Assoc Hydrol Sci. 224.

- 545 12. Clotet, N.; Gallart, F. Sediment yield in a mountainous basin under high mediterranean climate; three  
546 years of research and future studies. *Z. Geomorphologie, Supplement*, 1986. 60, 205-216.
- 547 13. Schumm, S.A. Evolution of drainage systems and slopes in badlands at Perth Amboy, New Jersey. *Bull*  
548 *Geol Soc Am* 1956. 87, 597-646.
- 549 14. Prout, H.A. A gigantic Paleotherium. *Am Jour Sci* 1846. 2(2), 288-289.
- 550 15. Evanoff, E.; Terry, D.O. Jr.; Benton, R.C.; Minkler, H. Field guide to geology of the White River Group in  
551 the North Unit of Badlands National Park. Field guide for Annual Meeting of the Rocky Mountain  
552 Region, Geological Society of America, Rapid City, SD, 2010; Terry, M.P.; Duke, E.F.; Tielke, J.A. Eds. SD  
553 School of Mines and Tech Bulletin 21, Geologic Field Trips in the Black Hills Region, South Dakota,  
554 U.S.A. 96-127.
- 555 16. Schumm, S.A. Erosion on miniature pediments in Badlands National Park, South Dakota. *Bull Geol Soc*  
556 *Am* 1962. 73(6), 719-724.
- 557 17. Stoffer, P.W. Geology of Badlands National Park: A preliminary report. OFR 03-358 U.S. Geological  
558 Survey, Menlo Park, CA, 2003.
- 559 18. Stetler, L.D.; Benton, R.; Weiler, M. Erosion Rates from Badlands National Park. Proceedings of the  
560 International Symposium on Erosion and Landscape Development, Anchorage, AK, U.S.A., 2011;  
561 American Society of Agricultural and Biological Engineers: St. Joseph, Missouri, U.S.A.
- 562 19. Stetler, L.D. Final Research Report: Determining Erosion Rates at Select Fossil Sites to Develop a  
563 Paleontological Monitoring Program. Technical Report FRR-063014, 2014. South Dakota School of Mines  
564 and Technology, Rapid City, SD, U.S.A., 222p.
- 565 20. US-Parks.com Inc. Badlands National Park. 2017. Available online: <http://www.us-parks.com> (accessed  
566 on 10 Dec 2017).
- 567 21. Van Houten, F.B. Clay minerals in sedimentary rocks and derived soils. *Am Jour Sci* 1953. 251, 61-82.
- 568 22. Smith, K.G. Erosional processes and landforms in Badlands National Monument, South Dakota. *Bul Geol*  
569 *Soc Am* 1958. 69, 975-1008.
- 570 23. Graham, J. Badlands National Park Geologic Resource Evaluation Report. Natural  
571 Resource Report NPS/NRPC/GRD/NRR, 2008. National Park Service, Denver,  
572 Colorado.
- 573 24. Howard, A.D. Badlands. In *Geomorphology of Desert Environments*. Abrahams, A.; Parsons, A.J. Eds.;  
574 Chapman & Hall, London, England, 1994; pp. 213-242. 978-94-015-8256-8.
- 575 25. Folk, R.L. *Petrology of Sedimentary Rocks*, Hemphill Publishing Company, Austin, Texas, U.S.A. 1980;  
576 182p. 0-914696-14-9.
- 577 26. Meng, I.S.T.S. Slope Stability Analysis (Revised April 06), Technical Note: SSP Geotechnics Sdn Bhd,  
578 Selangor, Malaysia, 2006. 32p.
- 579 27. Fredlund, D.G.; Krahn, J. Comparison of slope stability methods of analysis. *Can Geotech Jour* 1977. 14,  
580 429-439.
- 581 28. Davis, W.M. The convex profile of bad-land divides. *Sci* 1892; 20, 245.
- 582 29. Howard, A.D. A study of process and history in desert landforms near the Henry Mountains, Utah. PhD  
583 dissertation, Johns Hopkins University, Baltimore, MD, U.S.A., 1970.
- 584 30. Carson, M. A. Models of hillslope development under mass failure. *Geograph Anal* 1969; 1, 77-100.
- 585 31. Lambe, T.W.; Whitman, R.V. *Soil Mechanics*. John Wiley and Sons: New York, NY, U.S.A., 1969; 553p.  
586 0471511927.

- 587 32. Carson, M. A.; Kirby, M.J. *Hillslope Form and Processes*. Cambridge University Press: New York, NY,  
588 U.S.A., 1972; 476p. 052108234X, 9780521082341.
- 589 33. Budhu, M. *Soil Mechanics and Foundations*, 3rd ed.; John Wiley and Sons: New York, NY, U.S.A., 2010;  
590 763p. 978-470-55684-9.
- 591 34. ASTM Standard. D-854 Standard Test Methods for Specific Gravity of Soil Solids by Water Pycnometer.  
592 2011. Available online: <http://www.astm.org> (accessed 10 June 2014).
- 593 35. Knighton, D. *Fluvial Forms and Processes, A New Perspective*. Oxford University Press: New York, NY,  
594 U.S.A., 1998. 383p. 0-340-66313-8.
- 595 36. Julien, P.Y. *River Mechanics*. Cambridge University Press: Cambridge, England, 2002; 434p.  
596 0-521-56284-8.
- 597 37. Utley, B.C.; Wynn, T.M.. Cohesive soil erosion: theory and practice. Proceedings of the World  
598 Environmental and Water Resources Congress 2008 Ahupua'a, Honolulu, HI, U.S.A., 2008; Babcock,  
599 R.W. Ed.; American Society of Civil Engineers: pp. 1-10.
- 600 38. Hjulström, F. Studies of the morphological activity of rivers as illustrated by the River Fyris. PhD  
601 dissertation, Uppsala Universitet, Uppsala, Sweden, 1935. 306p.
- 602 39. Shields, A. Application of similarity principles and turbulence research to bed-load movement.  
603 Translated by Ott, W.P.; Van Uchelen, J.C., Soil Conservation Service, Cooperative Laboratory,  
604 California Institute of Technology, Pasadena, CA, U.S.A. 1936. 47p.
- 605 40. Bagnold, R.A. *The Physics of Blown Sand and Desert Dunes*. Methuen and Co., Ltd.: London, England,  
606 1941: 265p.
- 607 41. Santamarina, J.C. Soil behavior at the microscale: particle forces. Proceedings of the Symposium on Soil  
608 Behavior and Soft Ground Construction, Boston, MA, 2002; Germaine, J.T.; Sheahan, T.C.; Whitman,  
609 R.W. Eds.; American Society of Civil Engineers Geotechnical Special Publication 119: pp. 25-56.
- 610 42. Chow, V.T. *Open Channel Hydraulics*. McGraw-Hill: New York, NY, U.S.A., 1959: 680p. 007085906X.